

Nonlinear Adaptive Observation of the Liquid Water Saturation in PEM Fuel Cells

Andreu Cecilia^{a,*}, Maria Serra^a, Ramon Costa-Castelló^a

^a*Institut de Robòtica i Informàtica Industrial, CSIC-UPC, Llorens i Artigas 4-6, 08028 Barcelona, Spain*

Abstract

Efficiency, reliability and lifetime of polymer electrolyte membrane fuel cells (PEMFCs) are significantly limited by inadequate water management. High-performance water active control algorithms cannot be implemented due to the absence of adequate online sensors that can measure the internal liquid water saturation. A promising technique that can be applied in this context is the state observer. However, fuel cell models present strong nonlinearities, model uncertainty, unmatched unknown parameters and sensor noise, which are major difficulties in observer design. The algorithm proposed in this work is based on a time-varying adaptive observer, that offers an estimation of the liquid water state and behaviour in the cathode catalyst layer of a PEMFC, coupled with a low-power peaking-free observer with dynamic dead-zone filtering that is used as a high-performance soft sensor. The algorithm is shown to provide an accurate estimation of the liquid water saturation and the liquid water transport parameters even in the presence of sensor noise and model inaccuracies. The results are validated through numerical simulations and in a real experimental prototype.

Keywords: Proton exchange membrane fuel cell (PEMFC), Catalyst layer, Liquid water, State estimation, Parameter estimation, Noise

1. Introduction

Hydrogen has been established as a key element to tackle the present critical energy challenges. However, to make a significant contribution to a clean energy transition, it is crucial that hydrogen is incorporated in strategic sectors as transport, buildings and stationary power generation. A promising device to promote such introduction are fuel cells. A hydrogen fuel cell is an electrochemical device that converts the chemical energy of hydrogen in DC current without relying on moving parts and emission of pollutants, which makes it a promising alternative to traditional internal combustion engines.

Among the different types of fuel cell, polymer electrolyte membrane fuel cells (PEMFC) have been established as the most promising fuel cell candidate in transport and stationary backup power applications, due to its low-operating temperature, high-energy density, quick start-up and zero to low emissions [1].

Nevertheless, degradation problems limit the economical and technological viability of PEMFCs [2]. Transport applications require variable operating conditions, which induces significant fluctuations in the fuel cell's internal states. Inadequate operating conditions and dynamics will eventually lead to performance and components degradation [3]. Some crucial internal variables are the ones related to the fuel cell's water content [4]. Water flooding and drying are adverse phenomena that have significant effects on the fuel cell output voltage, performance and degradation [5]. In order to avoid such conditions, it is required to develop external humidification active control algorithms that

ensure adequate hydration, which presents a challenging problem. First, external humidifiers usually present slow dynamic response attributed to the temperature exchange process of the humidified gas and dry gas; thus, poor designed control algorithms will lead to over/under humidification. Second, fuel cell systems are related to highly nonlinear, delayed and uncertain processes. As a consequence, hydration control requires the development of advanced high-performance controllers, e.g. sliding mode controllers [6], nonlinear output-feedback linearization [7] or backstepping designs for time delayed systems [8], between others, which rely on having an accurate measurement of the PEMFC's water state. Therefore, a limiting factor in PEMFC water management is the existence of feasible internal humidity sensors.

External relative humidity sensors can only measure the vapour pressure of the inlet and outlet gases, which is not directly related to the fuel cell's water content and cannot measure liquid water. More complex measuring techniques as the current distribution method [9], neutron radiography [10] or x-ray radiography [11], are far too expensive, slow and intrusive to be a viable option for feedback loops in transport applications. The membrane water content can be estimated by analyzing the high-frequency components of the fuel cell spectral impedance [12]. However, such study requires the use of the electrochemical impedance spectroscopy technique or the feedback relay technique [13], which significantly modifies the operation of the fuel cell during the parameter estimation.

In such conflict, a viable approach is to develop online estimation algorithms of the liquid water content inside the fuel cell. In the context of feedback control, a useful estimation method is the state observer. The main reason is that the stability of the controller and observer coupling can be proved applying well-

*Corresponding author.

Email address: andreu.cecilia@upc.edu (Andreu Cecilia)

understood dynamic systems theory. This property may not hold for alternative types of estimators. Moreover, such alternative estimators may present long computation times, which reduces the bandwidth of the estimator dynamics [14]. Therefore, the design of fuel cell observers is a central topic for fuel cell water active control and fuel cell optimal management.

The aim of this work is to develop an observer algorithm to estimate the liquid water content of a PEMFC. The objective is simple but its execution presents significant issues that have to be addressed. First, fuel cell dynamics are highly nonlinear. A simple solution to such issue is to approximate the system by taking the first order elements of the Taylor expansion, and then, implementing a linear observer in the resulting dynamics. A prominent example of such technique is the Extended Kalman Filter (EKF). However, such approach assumes that the higher order terms of the Taylor expansion obeys a Gaussian distribution. In doing so, additional model errors are being introduced, as this assumption is not satisfied in the entire PEMFC model's uncertainty domain. This fact explains the low accuracy and reduced stability of EKFs in electrochemical systems [15]. As a consequence, higher performance can be obtained through the design of a nonlinear observer. Second, fuel cell models present significant uncertainty. There are still significant unknowns in the field of control-oriented fuel cell modelling and identification. Therefore, unavoidable discrepancy between the model and reality is expected to be found. This fact has motivated the implementation of robust observers in the PEMFC field [16–18]. Nonetheless, such approach provides limited information of the model uncertainty, which could be useful for diagnostics purposes. Third, due to technological and economical constraints, fuel cell temperature and pressure sensors present significant unknown high-frequency noise. It is well-known that the presence of sensor noise limits the robustness and convergence rate of an observer [19]. Thus, observers should be designed taking into account the noise presence.

For this reason, this work will present a new observer structure that can deal with nonlinearities, uncertainty and noise. The observer will be based on techniques for Lipschitz systems [20], which can deal efficiently with PEMFC model nonlinearities. The observer is coupled with a gradient-descent like parameter estimator to achieve an estimation of the unknown liquid water dynamics' parameters, following well-known adaptive observer ideas [21]. It is shown that such observer can only be implemented under a restrictive parameter/output matching condition, which is not satisfied in the considered system. To circumvent this limitation, the proposed adaptive observer is coupled with a high-gain observer that is used as a soft sensor to estimate an auxiliary signal, z , that satisfies the matching condition. Finally, the high-gain observer is modified by combining the ideas of the peaking-free observer [22] and dynamic dead-zone filtering [23] in order to out-perform classic high-gain techniques and reduce its noise sensitivity. A general scheme of the proposed strategy is depicted in Fig. 1.

The specific contributions of this work are:

- Propose a nonlinear adaptive observer that achieves an accurate estimation of the liquid water saturation in the

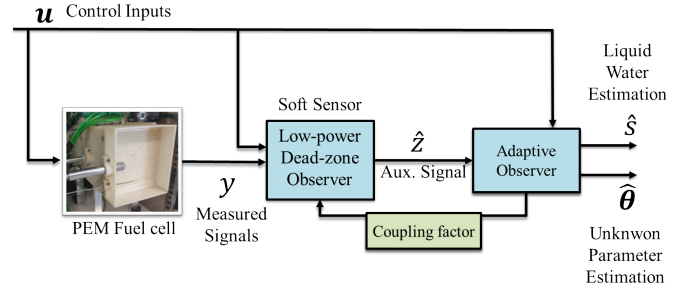


Figure 1: Scheme of the proposed observer for PEMFC

cathode catalyst layer (CCL) of a PEMFC, taking into account model uncertainty, unmatched unknown parameters and sensor noise.

- Couple the observer with a parameter estimation dynamics that achieves an estimation of the unknown absorption/desorption coefficient, liquid water evaporation rate and liquid water diffusion coefficient.
- Propose a whole observer scheme that, by means of a soft sensor, is able to fulfil the parameter/output matching condition, which is ubiquitous in adaptive observer problems.
- Validate the proposed estimation scheme through numerical simulations and experimental validation, where sensor noise and uncertainty are taken into account.

The remaining of this paper is organized as follows. Section 2 introduces a PEMFC model that will be used to design the observer. Section 3 formulates the estimation problem. Section 4 introduces an adaptive observer for the estimation of the liquid water saturation and the unknown parameters related to the liquid water dynamics. Section 5 validates the observer in a numerical simulation. Section 6 validates the technique in a real experimental prototype. Finally, some conclusions are drawn in Section 7.

2. PEMFC state space model

In the literature, there are plenty of PEMFC physical models, the accuracy and computational complexity of which depends on the desired application [4]. This work considers a two-phase flow non-isothermal lumped parameter model of an air-feed open-cathode PEMFC's CCL [24][25]. The model solves the heat equation, in the whole fuel cell stack and assumes a uniform temperature distribution to solve for the CCL's temperature, T_{fc} . Furthermore, the model solves the liquid water dynamics equation in the CCL, taking the membrane and the gas diffusion layer as boundaries. Specifically, the model considers the liquid water saturation in the CCL, s , which is defined as the volume fraction of liquid water in the pores. This allows to write the system equations in the following lumped parameter state-space

form

$$\begin{aligned}\dot{\mathbf{x}} &= \mathbf{f}_s(\mathbf{x}, I) + \mathbf{g}(\mathbf{x})v_{air} \\ y &= T_{fc} + v.\end{aligned}\quad (1)$$

The state vector, \mathbf{x} , is defined as: $\mathbf{x} = [T_{fc}, s]^T$; and the control inputs are the load current and the cathode air velocity, $\mathbf{u} = [I, v_{air}]^T$.

Moreover, the vector functions \mathbf{f}_s , \mathbf{g} are:

$$\mathbf{f}_s(\mathbf{x}, I) = \begin{bmatrix} K_1(E_{th}n_{cell} - V_{fc})I \\ \frac{1}{K_s}(K_3I - \frac{K_{evap}}{A_{pore}}K_4f_p(T_{fc}, s)) - K_5f_d(s) \end{bmatrix}$$

$$\mathbf{g}(\mathbf{x}) = \begin{bmatrix} K_2(T_{amb} - T_{fc}) \\ 0 \end{bmatrix}$$

with E_{th} [V] being the theoretical potential, n_{cell} the number of cells in the stack, V_{fc} [V] is the stack voltage computed through (2), K_s [$kg\ m^{-2}$] is the ionomer sorption/desorption coefficient, K_{evap} [$m^3\ s^{-1}$] is the evaporation time constant, A_{pore} [$m^2\ m^{-3}$] is the effective pore surface area per unit volume.

The constants K_1, \dots, K_5 are defined as:

$$K_1 = \frac{1}{m_{fc}C_{p,fc}}, \quad K_2 = \frac{\rho_{air}A_{inlet}C_{p,air}}{m_{fc}C_{p,fc}},$$

$$K_3 = \frac{M_{H_2O}}{2FA_{geo}}, \quad K_4 = \frac{M_{H_2O}}{R},$$

$$K_5 = \sigma \cos \Theta \sqrt{\epsilon K_{eff}} \frac{\rho_l}{K_s \mu_l \delta_{CL,c}},$$

where m_{fc} [kg] is the stack's mass, $C_{p,fc}$ [$J\ kg^{-1}\ K^{-1}$] is the fuel cell averaged heat capacity, ρ_{air} [$kg\ m^{-3}$] is the cathode air density, A_{inlet} [m^2] is the cathode housing cross-sectional area, $C_{p,air}$ [$J\ kg^{-1}\ K^{-1}$] is the cathode's air heat capacity, the factor ρC_p [$J\ K^{-1}\ m^{-3}$] is the specific heat capacity of the fuel cell stack, M_{H_2O} [$kg\ mol^{-1}$] is the molar mass of water, F [$C\ mol^{-1}$] is the Faraday constant, R [$J\ K^{-1}\ mol^{-1}$] is the ideal gas constant, σ [$N\ m^{-1}$] is water's surface tension, Θ [$^\circ$] is the effective contact angle in the diffusive media, ρ_l [$kg\ m^{-3}$] is the liquid water density, μ_l [$kg\ m^{-1}\ s^{-1}$] is the water dynamic viscosity and $\delta_{CL,c}$ [m] is the CCL's width.

The nonlinear functions f_p and f_d are computed as:

$$f_p(T_{fc}, s) = \frac{s}{T_{fc}}(p^0 e^{-E_a/(k_b T_{fc})} - p_v),$$

$$f_d(s) = s^3(1.42(1-s) - 2.12(1-s)^2 + 1.26(1-s)^3)$$

where E_a [eV] is the activation energy of the evaporation, the factor k_b [eV K^{-1}] is the Boltzmann parameter, p^0 [Pa] is a pre-exponential factor and p_v [atm] is the water vapour pressure in the CCL.

The model also includes a static relation between the system states, \mathbf{x} , and the fuel cell output voltage, V_{fc} , where activation and ohmic losses are considered. Specifically, the voltage is computed as:

$$V_{fc} = n_{cell}(E_{th} - \eta_{act} - \eta_{ohm}). \quad (2)$$

The factor η_{ohm} depicts the ohmic losses which are computed through the ohm's law,

$$\eta_{ohm} = R_{ohm}I$$

where R_{ohm} accounts for the ionic conductivity of the membrane and the resistance of the fuel cell's electric conductive components.

The factor η_{act} accounts for the activation losses which is computed as:

$$\eta_{act} = \frac{RT_{fc}}{2\alpha F} \ln\left(\frac{I}{A_{geo}j_0}\right)$$

where α is the transfer coefficient. The factor j_0 depicts the exchange current density which is corrected taking into account the effect of the temperature and liquid water saturation in the CCL with respect to the reference conditions [24],

$$j_0 = 0.21 j_0^{ref} a_c \left(1 - \left(\frac{s_{opt} - s}{s_{opt}}\right)^{1/3}\right) e^{\left(\frac{-\Delta G^*}{RT_{fc}} \left[1 - \frac{T_{fc}}{T_{ref}}\right]\right)}$$

where j_0^{ref} [$A\ m^{-2}$], a_c [-] and T_{ref} [K] are the reference exchange current, electrode rugosity and stack temperature, respectively, at a reference operating conditions. s_{opt} [-] is the liquid water saturation in which the effective $ECSA$ is maximum.

It should be remarked that, in the following sections, the signal that is going to be used to estimate the states, is the fuel cell stack temperature, $y = T_{fc} + v$, where v depicts high-frequency sensor noise. An alternative option is to use the stack voltage, V_{fc} , as the measured variable. However, there are some reasons that discourages such choice. First, the observability map from the stack voltage present singularities, i.e. there are operating points where the state cannot be reconstructed from V_{fc} . Second, PEMFCs that operate in dead-end mode have to periodically purge the anode due to the accumulation of inert gases or water [12], which induces some unmodelled perturbations on the stack voltage and can significantly affect the estimation performance. On the contrary, these purges do not have a significant effect on the fuel cell temperature, T_{fc} .

3. Problem formulation and observer objectives

The main objective is to design an estimator that might be used in a feedback loop, in which, depending on the type of application, different observer's performances are required. This work does not focus on the control application; thus, some generic performance objectives will be established.

First, the main objective of the observer is to achieve an accurate estimation of the liquid water saturation, \hat{s} , despite the presence of sensor noise and model uncertainty. In this work, an estimation is going to be accepted as accurate if the relative error converges, after some time, to a value below the 5%¹.

Second, there exist methodologies to accurately measure or estimate the parameters K_1, \dots, K_4 [24]. However, the estimation

¹The relative error [%] between \mathbf{x} and $\hat{\mathbf{x}}$ is computed as $\frac{\|\mathbf{x} - \hat{\mathbf{x}}\|}{\|\mathbf{x}\|} \cdot 100$

of K_5 (liquid water diffusion coefficient), K_{evap} (evaporation time constant) and K_s (absorption/desorption coefficient) is still and open problem, which introduces significant uncertainty in the liquid water equation. Moreover, these parameters are strongly dependent on the operating conditions [4]. Therefore, another objective of the observer will be to achieve an accurate estimation of the unknown parameters, \hat{K}_5 , \hat{K}_{evap} and \hat{K}_s for an arbitrary operating point. For the rest of the document, the unknown parameter vector will be referred as

$$\boldsymbol{\theta} = \left[\frac{1}{K_s}, \quad \frac{K_{evap}}{K_s A_{pore}}, \quad K_5 \right]^T.$$

Remark 3.1. The parameter θ_1 is defined as $\frac{1}{K_s}$ instead of the natural K_s . The motivation behind such parameterization is that the resulting model is linear with respect to the parameter vector $\boldsymbol{\theta}$, which eases the adaptive observer design. Furthermore, the parameter θ_2 depends on A_{pore} , which is assumed to be known. This definition avoids the numerical ill covariance matrix that is obtained if A_{pore} is not included in the parameter vector.

As a final objective, the observer needs to be fast enough so the observer and the future feedback controller can be designed separately. Fuel cell's water dynamics require around between 400 and 1000 seconds to reach an equilibrium point [4]. It will be assumed that the observer is adequate if it can reach an accurate estimation within the first 200 seconds. No time performance is required for the parameter estimation.

4. High-gain based Adaptive Observer

The whole observer scheme is based on the following adaptive observer result.

4.1. Adaptive observer

Define the auxiliary signal $z \triangleq T_{fc} + s = \mathbf{h}^T \mathbf{x}$, and consider the following state estimation dynamics,

$$\dot{\hat{\mathbf{x}}} = \mathbf{A}(\mathbf{u})\hat{\mathbf{x}} + \mathbf{f}(\hat{\mathbf{x}}, \mathbf{u}) + \mathbf{B}\boldsymbol{\phi}(\hat{\mathbf{x}}, \mathbf{u})\hat{\boldsymbol{\theta}} + \mathbf{k}(z - \mathbf{h}^T \hat{\mathbf{x}}) \quad (3)$$

$$\dot{\hat{\boldsymbol{\theta}}} = -\sigma \mathbf{P} - \mathbf{A}(\mathbf{u})^T \mathbf{P} - \mathbf{P} \mathbf{A}(\mathbf{u}) + \mathbf{h} \mathbf{h}^T \quad (4)$$

where $\hat{\mathbf{x}}$ is the estimation of the states \mathbf{x} , σ is a positive design parameter and

$$\mathbf{k} = \mathbf{P}^{-1} \mathbf{h}. \quad (5)$$

Moreover,

$$\boldsymbol{\phi}(\mathbf{x}, \mathbf{u}) = \left[\phi_1(\mathbf{u}), \quad \phi_2(\mathbf{x}), \quad \phi_3(\mathbf{x}) \right]$$

$$\mathbf{f}(\mathbf{x}, \mathbf{u}) = \begin{bmatrix} \mathbf{f}_1(\mathbf{x}, \mathbf{u}) \\ 0 \end{bmatrix}$$

$$\mathbf{A}(\mathbf{u}) = \begin{bmatrix} -K_2 v_{air} & 0 \\ 0 & 0 \end{bmatrix}; \quad \mathbf{B} = \begin{bmatrix} 0 \\ 1 \end{bmatrix}$$

where

$$\begin{aligned} f_1(\mathbf{x}, \mathbf{u}) &= K_1(E_{th} n_{cell} - V_{fc})I + K_2 T_{amb} v_{air} \\ \phi_1(\mathbf{u}) &= K_3 I, \quad \phi_2(\mathbf{x}) = -K_4 f_p(T_{fc}), \quad \phi_3(\mathbf{x}) = -f_d(s). \end{aligned}$$

The first elements of (3) can be interpreted as a copy of the original system (1) plus a linear injection term, $\mathbf{k}(z - \mathbf{h}^T \hat{\mathbf{x}})$, that is going to correct the state estimation according to the estimation error, $z - \mathbf{h}^T \hat{\mathbf{x}}$. The gain, \mathbf{k} , of this injection term is adapted according to the second dynamics (4) through expression (5), which allows to prove the stability of the estimation even with time-varying cathode air velocity, v_{air} , provided that σ is sufficiently large. This property may not hold for other observer gains [26]. Moreover, it achieves better performance in terms of robustness and noise rejection than constant gain estimators.

The factor $\hat{\boldsymbol{\theta}}$ depicts the estimation of the unknown parameters. This estimation is achieved through the following gradient descent-like dynamics

$$\dot{\hat{\boldsymbol{\theta}}} = \gamma \boldsymbol{\phi}(\hat{\mathbf{x}}, \mathbf{u})^T \mathbf{B}^T \mathbf{k}^\dagger (z - \mathbf{h}^T \hat{\mathbf{x}}), \quad (6)$$

where $\gamma > 0$ and \mathbf{k}^\dagger is the left Moore-Penrose pseudoinverse computed as:

$$\mathbf{k}^\dagger = (\mathbf{k}^T \mathbf{k})^{-1} \mathbf{k}^T.$$

Fig. 2 depicts an scheme of the proposed adaptive observer.

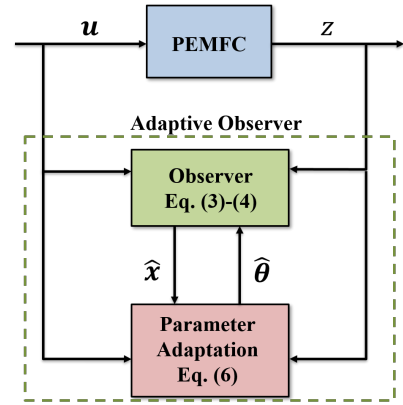


Figure 2: Adaptive observer for the PEMFC general scheme.

Now it is possible to establish the following.

Lemma 4.1. Consider system (1) and define $v_{air,max}$ as the maximum cathode air velocity. Then, there exists a positive value σ^* such that, for $\sigma > \max\{2v_{air,max}, \sigma^*\}$, the state estimation, $\hat{\mathbf{x}}$, of system (3)-(4) converges to the true value, \mathbf{x} provided that $v_{air} > 0$. Moreover, the parameter estimation, $\hat{\boldsymbol{\theta}}$, of (6) converges to the true value provided that the original system satisfies the following excitation condition for all $t > 0$

$$\mu_1 \mathbf{I} \geq \int_t^{t+T_0} \boldsymbol{\phi}(\tau)^T \mathbf{B}^T \mathbf{B} \boldsymbol{\phi}(\tau) d\tau \geq \mu_2 \mathbf{I}. \quad (7)$$

where μ_1 , μ_2 and T_0 are some positive constants

Intuitively, Lemma 4.1 establishes that, for a high enough term σ , the adaptive observer (3)-(6) achieves an exact estimation of the liquid water saturation, s , independently of the knowledge of the absorption/desorption, evaporation and diffusion coefficients. This is a stronger result than the one obtained

through robust observers as the high-gain observer [27] and/or the sliding mode observer [18]. Such observers can only reduce (not cancel) the effect of parameter uncertainty, and its accuracy relies on increasing the gain or the switching frequency of the injection term, which significantly increases the observer's sensitivity to sensor noise.

Remark 4.1. *The exact reconstruction property requires a non-zero cathode air velocity, as this condition is required for the observability of the system. Nonetheless, this condition is generally satisfied as some cathode air velocity is always required in order to deliver the necessary reactants to the CCL.*

Furthermore, Lemma 4.1 establishes a second result. If the regressor vector, ϕ , satisfies the excitation condition (7), i.e. the system trajectories are rich enough so that the gradient-descent algorithm (6) correctly interpolates the true system dynamics, the parameter estimation also converges to the true value. Notice that this excitation condition is not required for the exact state estimation. Nonetheless, the knowledge of the true model parameters could be used to assess the system performance and/or for diagnostics purposes, between others.

An interesting element in the adaptive observer structure is the use of the auxiliary signal z . In classic adaptive observers, the common approach is to implement a linear injection term that depends on the measured output error, i.e. $y - \mathbf{c}^T \hat{\mathbf{x}}$ [21], which in the considered problem would be $T_{fc} - \hat{x}_1$. Nevertheless, this output error-based adaptive observer is stable only if all the unknown model parameters appear in the first derivative of the output equation [21]. This assumption is referred as the matching condition, and is not satisfied in the concerned problem, as all the water dynamics' unknown parameters appear in the second derivative of the temperature function. For this reason, the proposed adaptive observer is coupled with a soft sensor to compute an auxiliary signal, z , that satisfies the matching condition in addition to all the required assumptions for the stability of the observer, as it is depicted in Fig. 1.

Notice that the auxiliary signal, z , cannot be directly computed, as the liquid water saturation, s , is an unknown variable. Thus, the main concern is to design an algorithm that can accurately estimate the auxiliary signal, \hat{z} . A high performance computation of \hat{z} can be achieved through a low-power observer with dynamic dead-zone filtering.

4.2. Low-power dead-zone observer

It is crucial to select the proper algorithm in order to build the proposed soft sensor. Not all algorithms that achieve an accurate auxiliary signal estimation can be implemented in the proposed estimation scheme. Indeed, there may be some algorithm that, in its own, achieves an estimation \hat{z} such that $\|z - \hat{z}\| \rightarrow 0$, but induces unstable dynamics once it is coupled with the adaptive observer (3)-(6).

In the concerned problem, the states that are required for the computation of the auxiliary signal z can be robustly estimated through a high-gain observer [27]. Moreover, it is possible to proof the stability of the whole estimation scheme through Lyapunov arguments [26]. Hence, the high-gain observer is

a good candidate for the soft sensor of the estimation scheme. However, the performance of high-gain observers is significantly affected by the peaking phenomena and the sensor noise, which is the main reason that discourages the implementation of high-gain observers in PEMFC systems [28]. Nevertheless, there has been some recent results in high-gain observation which have practically solved the peaking phenomena problem and has drastically reduced the effect of measurement noise. The combination of these results not only allows to reliably compute the auxiliary signal, z , in the presence of model uncertainty and sensor noise; but allows the implementation of high-gain observer based control techniques in fuel cells.

The mentioned results are twofold. First, the development of low-power peaking free observers [22], which eliminates the peaking phenomena and reduces the noise sensitivity while maintaining the convergence rate and robustness properties of classic high-gain observers. Second, the inclusion of dynamic dead-zones in the observer error injection terms [23], which allows filtering part of the sensor noise while achieving higher transient performances compared to observers that implements simple low-pass filters [27]. This work proposes combining both ideas in order to significantly out-perform the classic high-gain observer.

The low-power dead-zone observer is going to be adapted to the estimation of the unknown parameters. This is referred to as the "coupling factor" in Fig. 1. The coupling between the soft sensor and the adaptive observer allows the state and parameter estimation error to converge to an unbiased value, which is not accomplished in similar strategies for output-feedback design [26]. Specifically, the proposed soft sensor is computed through the following dynamics,

$$\begin{aligned}\dot{\hat{\xi}}_1 &= \eta_1 + \psi_1(\hat{\xi}_1, \mathbf{u}) + \frac{\alpha_1}{\varepsilon} dz_{\sqrt{\sigma_1}}(e_1) \\ \dot{\hat{\xi}}_2 &= \psi_2(\hat{\mathbf{x}}, \mathbf{u}, \hat{\boldsymbol{\theta}}, \dot{I}) + \frac{\alpha_2}{\varepsilon} dz_{\sqrt{\sigma_2}}(e_2) \\ \dot{\eta}_1 &= \psi_2(\hat{\mathbf{x}}, \mathbf{u}, \hat{\boldsymbol{\theta}}, \dot{I}) + \frac{\beta_1}{\varepsilon^2} dz_{\sqrt{\sigma_1}}(e_1)\end{aligned}\quad (8)$$

where $\alpha_1, \alpha_2, \beta_1$ and ε are parameters to be tuned [22], $\hat{\mathbf{x}}$ is the state estimation generated by the adaptive observer (3), and

$$\begin{aligned}e_1 &\triangleq y - \hat{\xi}_1, \\ e_2 &\triangleq sat_{r_2}(\eta_1) - \hat{\xi}_2.\end{aligned}$$

The nonlinear functions ψ_1 and ψ_2 are Lipschitz functions and defined as follows:

$$\begin{aligned}\psi_1(\hat{\xi}_1, \mathbf{u}) &= K_2(T_{amb} - \hat{\xi}_1)v_{air} \\ \psi_2(\hat{\mathbf{x}}, \mathbf{u}, \hat{\boldsymbol{\theta}}, \dot{I}) &= -IK_1 \frac{\partial V_{fc}}{\partial \mathbf{x}} \mathbf{f}_s(\hat{\mathbf{x}}, \hat{\boldsymbol{\theta}}, \dot{I}) - K_1 V_{fc} \dot{I}.\end{aligned}$$

The factor $dz_{\sqrt{\sigma}}(\cdot)$ is the dead-zone function computed as

$$dz_{\sqrt{\sigma}}(a) = a - sat_{\sqrt{\sigma}}(a)$$

where $sat_{\sqrt{\sigma}}(a)$ is the saturation function with amplitude $\sqrt{\sigma}$, which satisfies

$$sat_k(s) = s \quad \forall |s| \leq k, \quad sat_k(s) = k \quad \forall |s| \geq k. \quad (9)$$

This amplitude is dynamically adapted through the following expression

$$\dot{\sigma}_i = -\frac{q_i}{\varepsilon^2} \sigma_i + p_i \|e_i\|^2, \quad i = 1, 2. \quad (10)$$

where q_i and p_i are positive parameters to be tuned [23].

The inclusion of this dead-zone with dynamic amplitude ensures the stability of the observer and adapts the non-linear filter to the value of the noise.

Finally, the auxiliary signal is estimated through the following expression,

$$\hat{z} = \Phi(\hat{\xi}, \mathbf{u})^{-1} \triangleq \hat{\xi}_1 + s_{opt} \left(1 - \left[1 - \frac{IA_{geo}^{-1}}{0.21 J_0^{ref} a_c \exp\left(\frac{\eta_{act} n \alpha F}{R \hat{\xi}_1} - \frac{\Delta G^*}{R \hat{\xi}_1} \left(1 - \frac{\hat{\xi}_1}{T_{ref}}\right)\right)} \right]^3 \right)$$

where the activation overpotential, η_{act} , is estimated as

$$\eta_{act} = \frac{\hat{\xi}_2}{K_1 I} - \eta_{ohm}.$$

In Fig. 3 it is depicted a general scheme of the auxiliary signal estimation.

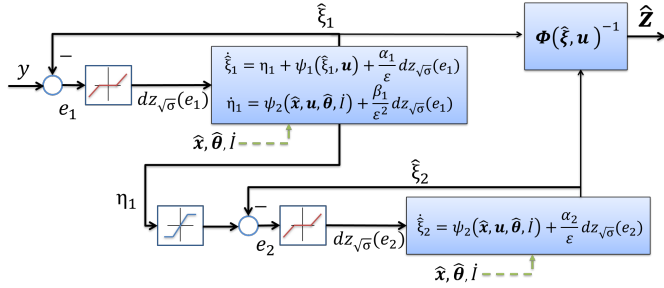


Figure 3: Scheme of the auxiliary signal estimation through a low-power peaking-free observer with dynamic dead-zone modification.

5. Numerical Simulations

In a numerical simulation, the model (1) is going to be excited with changes in the current signal, I , which will induce a stack temperature profile, T_{fc} , that will be used by the proposed observer scheme in order to estimate the liquid water saturation, s and the unknown parameters, θ . The model will use the parameters fitted in a real PEMFC with the values of K_s , K_{evap} and K_5 reported in [25]. The values of the parameters are summarized in Table A.4.

Nevertheless, from the observer point of view, it is assumed that there is no prior information of the unknown states and parameters. Therefore, the parameter estimation is initialized at zero, $\hat{\theta} = [0, 0, 0]^T$ and the state estimation is initialized at an arbitrary feasible operating condition $\hat{T}_{fc} = 300$ and $\hat{s} = 0.01$.

In reference to the current profile, the signal has been designed to be exciting enough so the system modes are active (in

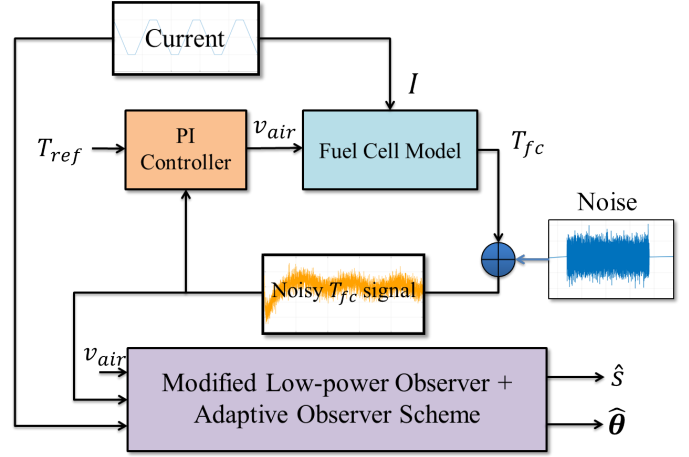


Figure 4: Simulation general scheme. The PI controller box depicts the temperature controller, the fuel cell model box depicts the model (1) with the parameters summarized in Table A.4 and the modified low-power observer+Adaptive observer scheme box depicts the proposed observer structure.

the sense of (7)) and not being too harsh that accelerates the degradation of the fuel cell. Moreover, the signal has been designed to be persistently exciting but, with lower excitation level (in the sense of having a lower μ_2 in (7)) than common PEMFC current profiles, which ensures that the proposed parameter estimation strategy can be replicated in a commercial PEMFC system during a real operation. Specifically, the current profile consists on a set of ramp functions between 3.8 A and 5 A with a slope of 0.006 A s^{-1} .

In order to make the simulation more realistic, two more elements have been included to the model. First, the temperature of the system will be controlled through a proportional integral controller (PI) that, through the cathode air velocity, v_{air} , will maintain the temperature close to a reference point, $T_{ref} = 304 \text{ K}$, despite the changes in the current profile. The observer is not used in this feedback loop, so, this document does not deal with the design of the controller. Second, the generated temperature profile is corrupted with random Gaussian noise with realistic variance value of 0.011 (taken from the real experimental set-up). The general scheme of the simulation is depicted in Fig. 4. The implementation of these two elements will make the stack temperature signal, which is the observer's main source of information, to vary very little from the reference point and this small variation will be mostly hidden by the sensor's noise, which is very common in PEMFC applications.

The observer's parameters have been designed to provide a state estimation settling time (98%) of 200 seconds and provide adequate noise rejection. Said parameters are summarized in the Table 1.

Moreover, it is assumed that there is no information of the current derivative, \dot{I} , required for the computation of $\psi_2(\hat{\xi}, \mathbf{u}, \theta, \dot{I})$. Therefore, the proposed observer has been implemented with $\psi_2(\hat{\xi}, \mathbf{u}, \theta, 0)$. This will induce some bias error in the estimation. It should be remarked that this bias can be significantly reduced by implementing a robust differentiator that estimates \dot{I}

Table 1: Adaptive observer parameters in numerical simulation

Parameter	Value
α_1	1.5
α_2	0.01
β_1	0.5
r_2	0.16
ε	0.11
σ	0.0612
γ	0.05
q_i	3
p_i	300

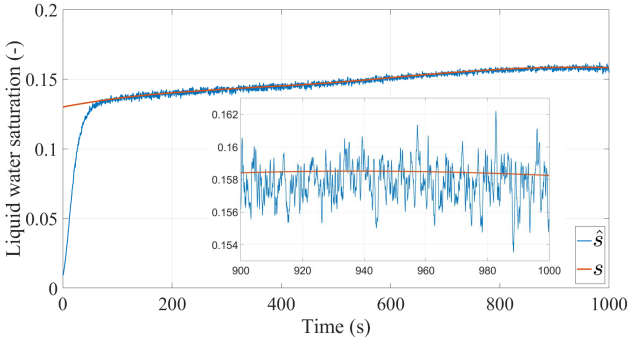


Figure 5: Model's liquid water saturation (orange) and adaptive observer's estimation (blue) in presence of measurement noise.

[29]. However, as it will be shown, the low-power peaking-free observer is robust with respect to the unmodelled \dot{I} , making the robust differentiator unnecessary.

The evolution of the model's true liquid water saturation and the observer's estimation is depicted in Fig. 5. The estimation error converges to a relative error below 3%, within the first 200 seconds. Therefore, the proposed scheme is capable of estimating the fuel cell CCL's liquid water saturation while satisfying the proposed observer performance objectives even in the presence of significant sensor noise. It is noticeable that there is a small bias between the estimation and the true value. This discrepancy is created by the absence of the factor \dot{I} in the observer equations. Nevertheless, the robustness of the low-power observer reduces the effect of the unknown \dot{I} , and the bias induced by this discrepancy is negligible.

The observer's estimation of the unknown parameters and the true model's values is depicted in Fig. 6. In all cases, after 200 seconds, the estimation converges to a relative error below 0.1% despite the presence of significant sensor noise and the unmodelled factor, \dot{I} . This convergence time is of the same time-scale as the PEMFC's water dynamics [4]. Thus, the estimation could be used for real-time fuel cell monitoring.

This numerical simulation shows that the proposed observer strategy is capable of estimating the PEM fuel cell liquid water saturation and unknown water dynamics parameters in a fast and robust manner despite that the stack temperature measurement is

nearly hidden by the noise. The desired observer objectives are quite generic, but the observer's parameters could be optimized to accommodate the observer to specific applications of control, identification or monitoring.

6. Experimental Validation

This section focuses on studying the performance of the proposed estimation scheme in a real experimental prototype.

6.1. Experimental set-up

This work considers a PEMFC stack H-100 of *Horizon fuel cell technologies* of 20 cells and a rated power of 100 W. Due to its small size, low weight and lack of peripherals (as a consequence of the open-cathode architecture) the PEMFC H-series are very attractive for small transport applications. The fuel cell's cathode is self-humidified and includes an attached fan that delivers air to the cathode and cools down the system. The cathode's air velocity is measured through a hot film sensor model EE75 of E+E Elektronik. The cathode's fan is controlled through a NI-9505 PWM module of National Instruments. Pure hydrogen is delivered in the anode side by a compressed air cylinder. In order to avoid the design of a flow controller, the H-100 fuel cell will be operated in dead-end mode [12]. A pressure regulator maintains the anode inlet pressure at 0.4 bar and 500 ms purges are executed every 20 seconds. Due to the open-cathode architecture, the PEMFC is fed with oxygen taken directly from the ambient air, which makes the system very sensible to the ambient conditions. In order to make the experiments reproducible, the fuel cell is enclosed in a environmental chamber that regulates the ambient temperature, relative humidity and oxygen concentration.

The humidity and ambient temperature at the cathode are measured through a sensor model HMM211 from Vaisala. Moreover, the temperature of each cell is measured, individually, through a type K thermocouple. The average of the 20 temperature measurements is taken as the averaged fuel cell stack temperature T_{fc} .

The experimental set-up includes a programmable load that allows to control the demanded current and emulate a real application. The stack voltage, V_{fc} , is measured through an isolation amplifier, model AD215 from Analog Devices and the exchange current, I , through a Hall effect sensor model LTS 6 NP of LEM.

The experimental set-up and a photography of the environmental chamber and the H-100 PEMFC can be seen in Fig. 7.

All the data acquisition devices are connected to a Compact Rio embedded controller cRIO-9047 of National Instruments, which includes a FPGA module and can be programmed in the *LabView* environment. All the data is acquired in a sampling time of two seconds, which is considered to be adequate, as the fuel cell thermal and water dynamics time scales are an order of magnitude larger and the observer computational cost is minimal at this frequency.

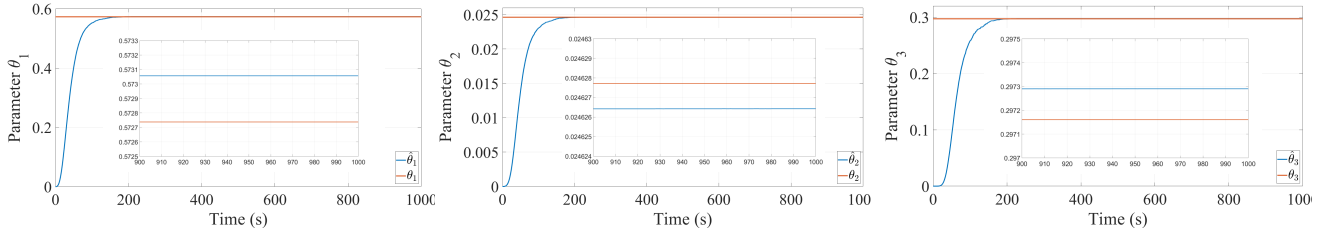


Figure 6: Model's unknown parameter θ true value (orange) and adaptive observer's estimation (blue) in presence of measurement noise.

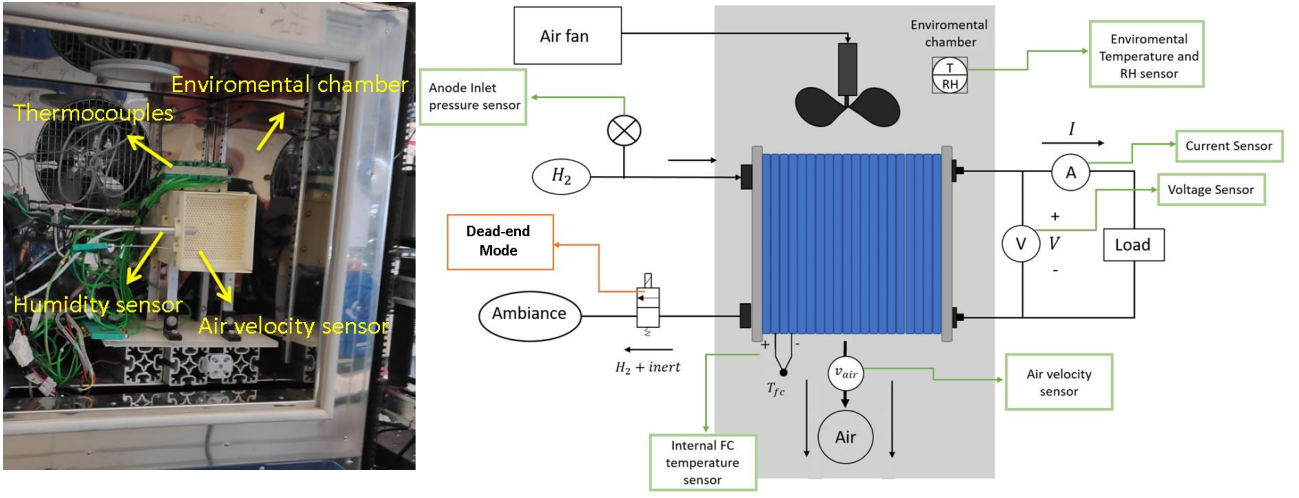


Figure 7: (a) Environmental chamber and H-100 PEMFC. (b) H-100 experimental set-up scheme.

6.2. Methodology

The main problem in validating the proposed observer strategy is the unavailability of liquid water saturation sensors. As a consequence, one can apply the proposed observer technique to generate an estimation of the water, \hat{s} , and the unknown parameters, but, these estimations cannot be compared with the true values. However, there exists other measured signals that can be used to endorse the estimation.

Specifically, the estimation of the stack temperature, \hat{T}_{fc} , the estimation of the liquid water saturation, \hat{s} , and the voltage equation (2) can be used to generate an estimation of the stack voltage, \hat{V}_{fc} . If we assume that there is sufficient air and hydrogen and the current is low enough, the fuel cell concentration losses are negligible. Thus, the accuracy of the stack voltage computation only depends on the stack temperature and the CCL's liquid water saturation, as seen in equation (2). Consequently, in such conditions, one can verify the accuracy of the liquid water saturation estimation by computing the errors $\|T_{fc} - \hat{T}_{fc}\|$ and $\|V_{fc} - \hat{V}_{fc}\|$.

The H-100 PEMFC setup will be excited by a constant exchange current of 3.9 A and a step function from 0.21 $m s^{-1}$ to 0.19 $m s^{-1}$ in the cathode's air velocity. As the current is maintained constant at a medium range value, it is not expected

to be significant water generation due to the cathode reduction reaction. However, due to the air velocity's decrease and the absence of temperature control, the fuel cell's stack temperature is expected to increase, which will boost the liquid water evaporation rates. Therefore, the CCL's liquid water saturation should reduce during the experiment, which should provide the necessary system excitation (7) for the parameter estimation.

The experiment conditions are summarized in Table 2.

Variable	Value	Units
Anode reactant	H_2	—
Cathode reactant	Ambient air	—
T_{amb}	25	$^{\circ}C$
RH_{amb}	75	%
Anode Pressure	0.4	Bar
Anode RH	0	%
Current	3.9	A

In order to assess if the system is truly persistently excited (7), in parallel, the integral (7) has been computed numerically as follows

$$\dot{Q} = -\kappa Q + \phi(\hat{x}, u)^T B^T B \phi(\hat{x}, u)$$

where \mathbf{Q} is a numerical computation of the integral (7), κ is the forgetting factor constant and \hat{x} is the observer's estimation of the states, which will be presented below.

The minimal eigenvalue of \mathbf{Q} is always positive in the experimental profiles. Thus, condition (7) is satisfied and the system is persistently excited.

6.3. System Identification

The H-100 fuel cell's parameters have been identified in the operating conditions depicted in Table 2 and in the corresponding stack temperatures. The system identification experiment consisted in introducing a step function in the cathode air velocity and measuring the stack temperature, T_{fc} , and voltage, V_{fc} . The temperature equation's parameters, K_1 and K_2 , have been fitted through a linear least squares of T_{fc} vs \hat{T}_{fc} , and the voltage equation's parameters R_{ohm} and α have been fitted through a linear least squares of V vs \hat{V}_{fc} . The values of j_0 and a_c have been taken from [25]. Reference values of the unknown parameters K_s , K_{evap} and K_5 are taken from [25]. These last three parameters will be used to assess the validity of the parameter estimation accuracy, but are not considered in the observer design and computation. The rest of the parameters are constants that have been taken from the literature. All these parameter values are summarized in Table A.4.

6.4. Results and discussion

The observer design parameters have been tuned to provide a state estimation settling time of 200 seconds and sufficient noise rejection, see Table 3. Moreover, again, it is assumed that there is no access to the derivative of the current. Thus, $\psi_2(\hat{\xi}, \mathbf{u}, \theta, \dot{I})$ is implemented as $\psi_2(\hat{\xi}, \mathbf{u}, \theta, 0)$.

Table 3: PEMFC observer parameters

Parameter	Value
α_1	1.5
α_2	0.01
β_1	0.5
r_2	0.15
ε	0.35
σ	0.219
γ	0.015
q_i	3
p_i	50

The constant current, the air velocity step profile and the induced stack temperature have been introduced in the proposed adaptive observer and, consequently, an estimation of the liquid water saturation has been generated, Fig. 8 (a). As stated before, the true value of the liquid water cannot be measured online, so, this estimation cannot be compared with any signal. Nevertheless, some conclusions can be drawn from this result.

In Fig. 8 (a), it can be noticed that the estimation converges to a value around 0.4, which is coherent with the optimal value s_{opt} depicted in Table A.4. Moreover, after the air velocity

change in second 325, it can be seen that the liquid water saturation has slowly decreased. This tendency was predicted during the experiment design, as an increase of the temperature results in an increase of the water evaporation rates.

Notice that the liquid water saturation estimation in Fig. 8 (a) stabilizes in the first 200 seconds, and, after the air velocity change, it stabilizes again in 200 seconds. Moreover, the high-frequency oscillations induced by the temperature sensor noise presents a peak-to-peak amplitude of less than 5%. It should be remarked that if a classic high-gain observer was applied as the soft sensor, this error would be significantly larger, and the estimation would be practically unusable.

In order to validate the accuracy of the estimation, the estimated stack temperature profile and liquid water saturation profile have been used to generate an estimation of the output voltage, \hat{V}_{fc} , through (2). As stated before, if \hat{V}_{fc} and \hat{T}_{fc} are accurate, then \hat{s} is also accurate. Moreover, the stack temperature and the output voltage have been measured. Therefore, addressing the accuracy of \hat{V}_{fc} and \hat{T}_{fc} is trivial. Specifically, the measured temperature profile and the observer's estimation is depicted in Fig. 8 (b). It can be seen that, after the transient, the relative error is below the 0.1%. The measured voltage evolution and observer's estimation is depicted in Figure 8 (c), where it can be seen that the voltage estimation converges to a relative error below the 0.4%. Following the reasoning presented in the methodology sub-section, as the temperature and voltage estimation converges to a relative error below the 0.4%, it can be concluded that the CCL's liquid water saturation estimation is also accurate.

In parallel to the liquid water saturation estimation, the adaptive observer has generated an estimation of the water dynamic's unknown parameters, θ . The accuracy of the observer's estimation has been assessed by direct comparison to the values reported in [25][24] for an H-100 fuel cell in similar operating conditions. It should be remarked that the values reported in [25][24] were not directly measured, but estimated through an off-line identification algorithm. Therefore, its validity should be treated carefully. Indeed, it will be shown that the values estimated through the observer proposed in this work presented higher prediction capabilities.

The evolution of the parameter estimation is depicted in Fig. 8 (d)-(f). It is noticeable that the estimation converges to a value of the same magnitude as the ones reported in [25][24], within the first 1000 seconds, which is in the timescale of the liquid water saturation dynamics [4]. It is noticeable the bias between the estimated value and the ones reported in previous works. This discrepancy is mainly explained by the algorithm that is used to estimate the parameters, K_5 , K_s and K_{evap} . In [25][24], these parameters were estimated through an off-line identification algorithm. Alternatively, this work has estimated these parameters through the on-line adaptation dynamics (6). It should be remarked that the values reported in [25][24], achieved a voltage estimation error of 0.5% and a temperature estimation error of 2%, which is significantly larger than the one reported in this work. Therefore, the parameters estimated through the proposed algorithm significantly improves the prediction capabilities of the model. Consequently, are closer to the optimal parameter

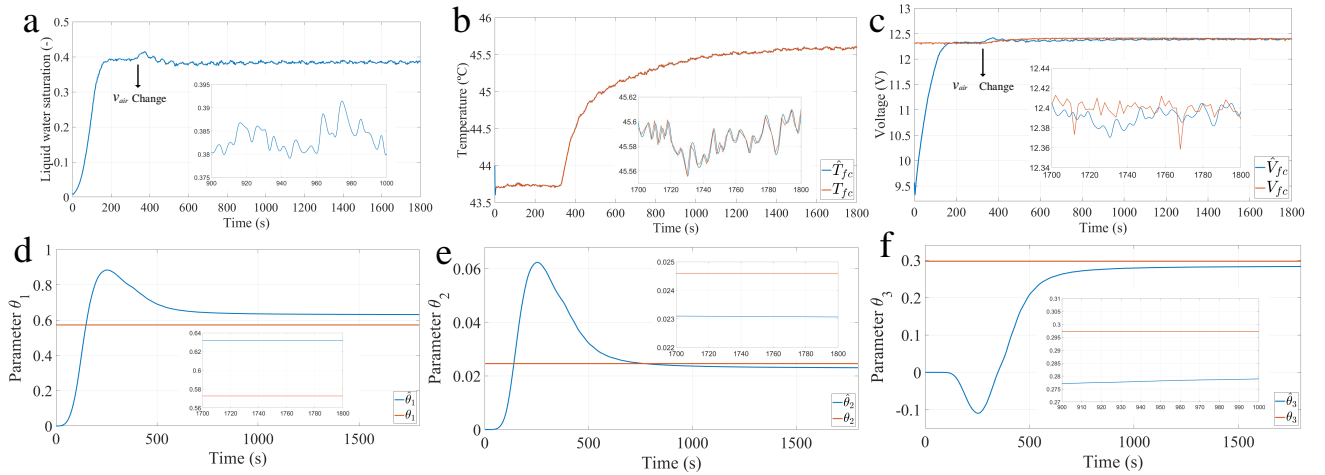


Figure 8: (a) Adaptive observer’s CCL liquid water saturation estimation. (b) Measured stack temperature profile (orange) and adaptive observer’s estimation (blue). (c) Measured stack temperature profile (orange) and adaptive observer’s estimation (blue). (d)–(f) Adaptive observer’s parameter estimation θ (blue) and parameter value estimated in [24][25] (orange). The values reported by the adaptive observer (blue) have achieved a more accurate voltage and temperature prediction than the ones estimated in [24][25]. Thus, are closer to the ideal parameter value in the studied experiment.

value.

7. Conclusions

This work has presented a new adaptive observer scheme for the problem of estimating the unknown states and parameters related to PEMFC CCL water dynamics based on a simple nonlinear model. Nonetheless, the state and parameter estimation problem presented significant obstacles and it was required to implement recent observer results to solve it. The proposed observer is based on a time-varying nonlinear adaptive observer. The relative degree assumption between the measured output and the unknown parameters, ubiquitous in adaptive observers, have been circumvented by coupling the adaptive observer with a high-gain observer as a soft sensor that estimates a certain auxiliary signal. The high-gain observer has been modified combining the ideas of low-power peaking free observation and dynamic dead-zone filtering which significantly improves the performance of this soft sensor. Finally, the technique has been validated through numerical simulations and in a real experimental set-up.

Nevertheless, this work presents some limitations that have to be addressed in future works. From the theoretical point of view, it could be interesting to modify the adaptive observer in order to relax the persistence of excitation condition (7), which may be too restrictive in certain operating points and may induce parameter bias in low excitation conditions. A promising approach is to modify the parameter adaptation dynamics with concurrent learning adaptive control ideas [30], which achieves an accurate parameter estimation under a weaker finite excitation condition.

Furthermore, in future works, the proposed fuel cell observer will be implemented in a set of control loops. A promising problem to be solved is the combination of the observer with

a path planning algorithm in order to make a water content-conscious control of PEM fuel cells in automotive planning problems.

CRedit authorship contribution statement

Andreu Cecilia: Conceptualization, Methodology, Software, Formal analysis, Writing- original draft, Writing- review & editing. **Maria Serra:** Supervision, Resources, Writing- review & editing. **Ramon Costa-Castelló:** Methodology, Project administration, Supervision, Writing- review & editing, Funding acquisition.

Declaration of competing interest

The authors declare that they have no known competing financial interests or personal relationships that could have appeared to influence the work reported in this paper.

Acknowledgement

This work has been partially funded by the Spanish State Research Agency through the María de Maeztu Seal of Excellence to IRI (MDM-2016-0656) and by the project DOVELAR (ref. RTI2018-096001-B-C32).

Appendix A. Parameters of the H-100 fuel cell

Table A.4 depicts the parameters of the H-100 fuel cell in the operating conditions depicted in table 2. The parameters K_s , K_{evap} and K_5 are from the study [25][24].

Table A.4: Parameters of the fuel cell model

Parameter	Value	Units
K_1	$3.276 \cdot 10^{-4}$	$K J^{-1}$
K_2	0.0255	m^{-1}
K_3	$4.1457 \cdot 10^{-5}$	$Kg C^{-1} m^{-2}$
K_4	0.0022	$Kg K J^{-1}$
E_{th}	1.44	V
T_{amb}	298	K
A_{geo}	0.00225	m^2
A_{pore}	$2.2E7$	m^2
p^0	1.196E11	Pa
E_a	0.449	eV
p_v	2380	Pa
n_{cell}	20	–
α	0.311	–
a_c	238	–
i_0^{ref}	$4.7E - 3$	$A m^{-2}$
ΔG^*	70000	$J mol^{-1}$
R_{ohm}	1.566	Ω
s_{opt}	0.55	–
k_b	$8.6170 \cdot 10^{-5}$	$eV K^{-1}$
R	8.314	$J K^{-1} mol^{-1}$
F	96485	$C mol^{-1}$
K_s	1.746	$Kg m^{-2}$
K_{evap}	$8.6E5$	$m^3 s^{-1}$
K_5	0.2972	s^{-1}

References

- [1] J. Lai, M. W. Ellis, Fuel cell power systems and applications, Proc. IEEE 105 (11) (2017) 2166–2190. doi:10.1109/JPROC.2017.2723561.
- [2] M. Jouin, R. Gouriveau, D. Hissel, M.-C. Péra, N. Zerhouni, Degradations analysis and aging modeling for health assessment and prognostics of pemfc, Reliab. Eng. Syst. Saf. 148 (2016) 78–95. doi:https://doi.org/10.1016/j.res.s.2015.12.003.
- [3] D. Zhao, F. Gao, P. Massonnat, M. Dou, A. Miraoui, Parameter sensitivity analysis and local temperature distribution effect for a pemfc system, IEEE Trans. Energy Convers 30 (3) (2015) 1008–1018. doi:10.1109/TEC.2015.2404793.
- [4] K. Jiao, X. Li, Water transport in polymer electrolyte membrane fuel cells, Prog. Energy Combust. Sci. 37 (3) (2011) 221–291. doi:https://doi.org/10.1016/j.peccs.2010.06.002.
- [5] O. Ijaodola, Z. [El-Hassan], E. Ogungbemi, F. Khatib, T. Wilberforce, J. Thompson, A. Olabi, Energy efficiency improvements by investigating the water flooding management on proton exchange membrane fuel cell (pemfc), Energy 179 (2019) 246–267. doi:https://doi.org/10.1016/j.energy.2019.04.074.
- [6] G. P. Incremona, M. Rubagotti, A. Ferrara, Sliding mode control of constrained nonlinear systems, IEEE Trans. Autom. Control 62 (6) (2017) 2965–2972. doi:10.1109/TAC.2016.2605043.
- [7] Y. Wu, A. Isidori, R. Lu, H. K. Khalil, Performance recovery of dynamic feedback-linearization methods for multivariable nonlinear systems, IEEE Trans. Autom. Control 65 (4) (2020) 1365–1380. doi:10.1109/TAC.2019.2924176.
- [8] F. Mazenc, P. Bliman, Backstepping design for time-delay nonlinear systems, IEEE Trans. Autom. Control 51 (1) (2006) 149–154. doi:10.1109/TAC.2005.861701.
- [9] J. Stumper, S. A. Campbell, D. P. Wilkinson, M. C. Johnson, M. Davis, In-situ methods for the determination of current distributions in pem fuel cells, Electrochim. Acta 43 (24) (1998) 3773–3783. doi:https://doi.org/10.1016/S0013-4686(98)00137-6.
- [10] A. Geiger, A. Tsukada, E. Lehmann, P. Vontobel, A. Wokaun, G. Scherer, In situ investigation of two-phase flow patterns in flow fields of pemfc's using neutron radiography, Fuel Cells 2 (2002) 92–98. doi:10.1002/fuce.200290007.
- [11] I. Manke, C. Hartnig, M. Grunerbel, W. Lehnert, N. Kardjilov, A. Haibel, A. Hilger, J. Banhart, H. Riesemeier, Investigation of water evolution and transport in fuel cells with high resolution synchrotron x-ray radiograph, Appl. Phys. Lett. 90 (Apr. 2007). doi:10.1063/1.2731440.
- [12] F. Barbir, PEM fuel cells: theory and practice, Academic Press, 2012.
- [13] F. Zenith, I. J. Halvorsen, I. Pivac, D. Bezmalinovic, F. Barbir, Electrochemical low-frequency impedance spectroscopy for diagnostics of fuel cells, in: IEEE Vehicle Power and Propulsion Conference (VPPC), 2019, pp. 1–5. doi:10.1109/VPPC46532.2019.8952402.
- [14] O. Aydogmus, M. F. Talu, Comparison of extended-kalman- and particle-filter-based sensorless speed control, IEEE Trans. Instrum. Meas. 61 (2) (2012) 402–410. doi:10.1109/TIM.2011.2164851.
- [15] J. Li, J. Klee Barillas, C. Guenther, M. A. Danzer, A comparative study of state of charge estimation algorithms for lifepo4 batteries used in electric vehicles, J. Power Sources 230 (2013) 244–250. doi:https://doi.org/10.1016/j.jpowsour.2012.12.057.
- [16] M. Benallouch, R. Outbib, M. Boutayeb, E. Laroche, Robust observers for a class of nonlinear systems using pem fuel cells as a simulated case study, IEEE Trans. Control Syst. Technol. 26 (1) (2018) 291–298. doi:10.1109/TCST.2017.2658181.
- [17] A. Pilloni, A. Pisano, E. Usai, Observer-based air excess ratio control of a pem fuel cell system via high-order sliding mode, IEEE Trans. Ind. Electron. 62 (8) (2015) 5236–5246. doi:10.1109/TIE.2015.2412520.
- [18] J. Luna, A. Husar, M. Serra, Nonlinear distributed parameter observer design for fuel cell systems, Int. J. Hydrog. Energy 40 (34) (2015) 11322–11332. doi:https://doi.org/10.1016/j.ijhydene.2015.05.132.
- [19] G. C. Goodwin, A critique of observers used in the context of feedback control, in: Z. Chen, A. Mendes, Y. Yan, S. Chen (Eds.), Intelligent Robotics and Applications, Springer International Publishing, Cham, 2018, pp. 1–24.
- [20] R. Rajamani, Observers for lipschitz nonlinear systems, IEEE Trans. Autom. Control 43 (3) (1998) 397–401.
- [21] Young Man Cho, R. Rajamani, A systematic approach to adaptive observer synthesis for nonlinear systems, IEEE Trans. Autom. Control 42 (4) (1997) 534–537. doi:10.1109/9.566664.
- [22] D. Astolfi, L. Marconi, L. Praly, A. R. Teel, Low-power peaking-free high-gain observers, Automatica 98 (2018) 169–179. doi:https://doi.org/10.1016/j.automatica.2018.09.009.
- [23] D. Astolfi, A. Alessandri, L. Zaccarian, Stubborn and dead-zone redesign for nonlinear observers and filters, IEEE Trans. Autom. Control (2020), to be published, DOI: 10.1109/TAC.2020.2989816).
- [24] S. Strahl, R. Costa-Castelló, Model-based analysis for the thermal management of open-cathode proton exchange membrane fuel cell systems concerning efficiency and stability, J. Process Control 47 (2016) 201–212. doi:https://doi.org/10.1016/j.jprocont.2016.09.004.
- [25] S. Strahl, A. Husar, P. Puleston, J. Riera, Performance improvement by temperature control of an open-cathode PEM fuel cell system, in: Fuel Cells, 2014. doi:10.1002/fuce.201300211.
- [26] A. Cecilia, M. Serra, R. Costa-castelló, PEMFC state and parameter estimation through a high-gain based adaptive observer, in: 21st IFAC World Congress, 2020.
- [27] A. Cecilia, R. Costa-Castelló, High gain observer with dynamic deadzone to estimate liquid water saturation in pem fuel cells, Rev. Iberoam. Autom. In. 17 (2) (2020) 169–180. doi:10.4995/riai.2020.12689.
- [28] H. Yuan, H. Dai, X. Wei, P. Ming, Model-based observers for internal states estimation and control of proton exchange membrane fuel cell system: A review, J. Power Sources 468 (2020) 228376. doi:https://doi.org/10.1016/j.jpowsour.2020.228376.
- [29] E. Cruz-Zavala, J. A. Moreno, Levant's arbitrary-order exact differentiator: A lyapunov approach, IEEE Trans. Autom. Control 64 (7) (2019) 3034–3039. doi:10.1109/TAC.2018.2874721.
- [30] H. Lee, H. Shin, A. Tsourdos, Concurrent learning adaptive control with directional forgetting, IEEE Trans. Autom. Control 64 (12) (2019) 5164–5170. doi:10.1109/TAC.2019.2911863.